2007 Fall Meeting of the Western States Section of the Combustion Institute
Sandia National Laboratories, Livermore, CA
October 16 & 17, 2007.

Effect of H_2O and NO on extinction and re-ignition of vortex-perturbed hydrogen flames in counterflow

Uen Do Lee, Chun Sang Yoo, Jacqueline H. Chen, and Jonathan H. Frank

Combustion Research Facility, Sandia National Laboratories

7011 East Ave, Livermore, CA 94551-0969, USA.

The influence of water vapor (H_2O) and nitric oxide (NO) on the extinction and re-ignition of a vortex-perturbed nonpremixed hydrogen-air flame is investigated. A steady nonpremixed flame is established in an axisymmetric counterflow configuration with a fuel stream of N_2-diluted H_2 flowing against heated air containing small amounts of H_2O and NO. Local flame extinction is induced by a fuel-side vortex, and the temporal evolution of the hydroxyl radical (OH) is measured during the extinction and re-ignition processes using planar laser-induced fluorescence (PLIF). It is well known that H_2O behaves as an inhibitor in combustion due to its high specific heat and that NO can significantly enhance the ignition of hydrogen due to its catalytic effect. In the present study, we investigate the sensitivity of extinction and re-ignition processes to mixtures of H_2O and NO. Direct numerical simulations are performed using a detailed H_2-air mechanism and are compared with experiments.

1. Introduction

An improved understanding of the complex coupling between transient flows and flame chemistry is important for the development of advanced combustion technologies with low pollutant emissions and stable operating conditions. In turbulent flames, intermittent fluctuations in transport rates can lead to localized flame extinction followed by re-ignition. This process is particularly challenging to model as mixed modes of combustion – ranging from autoignition of reactants mixed with intermediates and products of combustion to partially-premixed flame propagation – may coexist during re-ignition. Hydrogen combustion provides a simple chemical system for investigating the interactions of transient flows and flame chemistry. Hydrogen is an important submechanism in hydrocarbon chemistry, important in controlling both high temperature radical branching and thermal explosion in high pressure, intermediate temperature conditions. Moreover, practical applications of hydrogen combustion have received renewed interest as a result of recent increases in fossil fuel costs and concerns about climate change [1]. For example, hydrogen-rich fuels are being considered in next generation gas turbine technologies for power generation.

The addition of hydrogen to hydrocarbon fuels provides a method for improving performance and reducing emissions of practical combustion devices. It is well known that adding hydrogen to most hydrocarbons increases the laminar burning velocity and the flammability limits [2,3], and a small amount of hydrogen addition in turbulent flames improves flame stability [4]. In combustion with preheated reactant flows, hydrogen addition significantly increases the

extinction strain rate of lean-premixed methane flames. The breakdown of hydrogen increases radical production rates which enhances methane ignition under conditions where it is otherwise impossible for the ignition of methane [5].

As a sole fuel, or as a controlling agent, the low lean-flammability limit of hydrogen allows for highly diluted and low temperature combustion. Moreover ignition of the diluted system is very sensitive to additives such as water [6,7] and NO [8–17]. Because water and NO are representative products of hydrogen-air combustion, various control strategies are possible by employing exhaust gas recirculation (EGR) to hydrogen related combustion systems. As a major product of combustion, water vapor affects the critical conditions for extinction and autoignition of a reactant mixture. The addition of water vapor lowers the temperature of a reaction zone, and hence makes the flame easier to extinguish and more difficult to ignite. The chemical inhibition of water vapor is attributed to the enhanced chaperon efficiency of water on the three body reaction $H + O_2 + M \Leftrightarrow HO_2 + M$. On the other hand, NO addition has a catalytic effect on the ignition process and it decreases the ignition temperature of hydrogen and hydrocarbon fuels [9–17]. For hydrogen, the impact of NO on kinetics has been well established as a catalyst which significantly alters the ignition process by turning the chain terminating steps related to HO_2 formation ($H + O_2 + M \Leftrightarrow HO_2 + M$) into chain-branching steps related to OH formation ($NO + HO_2 \Leftrightarrow NO_2 + OH$, $NO_2 + H \Leftrightarrow NO + OH$) [8–12,15–17]. Practically, the catalytic effect of NO and the inhibition effect of water on ignition can be used to enlarge the lean flammability limit for low loads or to increase the power density for high loads by controlling the onset of low temperature combustion in HCCI engines.

In the present study, the effects of water and NO on the extinction and re-ignition of hydrogen flames are investigated using vortex-perturbed hydrogen diffusion flames. The oxidizer stream is heated to temperatures above the autoignition limit, and localized extinction is induced by an impulsively driving a fuel-side vortex into the flame. The extinction and recovery process of the flame are monitored in time with OH PLIF. The influence of water on the extinction and re-ignition process is investigated as a function of water mole fraction with and without NO addition. The vortex strength, air temperature and initial strain rate are kept constant for all experiments. Addition of a small amount of water vapor and NO in the hot oxidizer stream significantly alters the re-ignition process. To understand the effect of water and NO, direct numerical simulations (DNS) are conducted in the same configuration as the experiment. The simulations employ detailed chemistry that includes a recently developed NO reaction mechanism [15,17]. The coupling between experiments and simulations enables the investigation of the chemical effects related to water vapor and NO and provides detailed insight into the interaction between transient flows and ignition process.

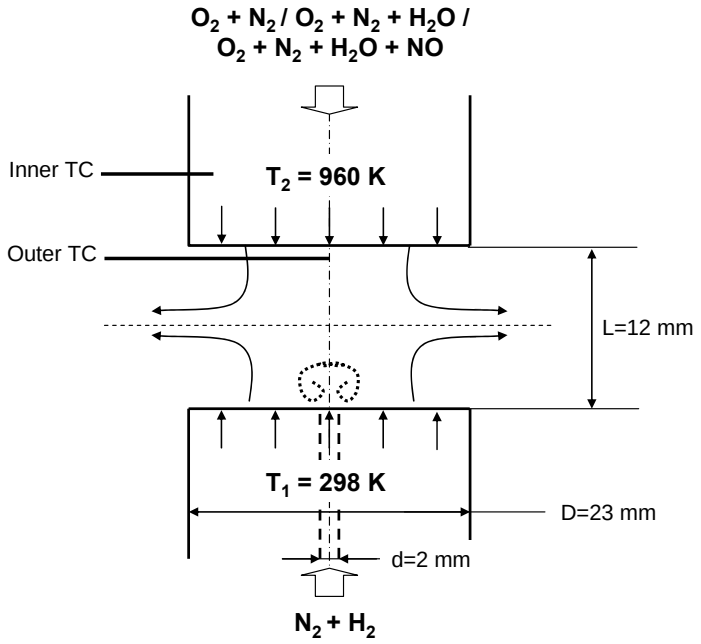

Figure 1: Counter-flow jets with an air-heating system

2. Experimental and Numerical Methods

2.1 Experimental method

Figure 1 shows the axisymmetric counter-flow burner equipped with a heating system in the top duct and a vortex generator in the bottom duct. Further details of the burner are given elsewhere [17]. The SiC heater inside the top duct is capable of heating the oxidizer flow up to a temperature of T_2 = 1300 K, and the oxidizer temperature is measured by the inner and outer thermocouples. In this experiment, the oxidizer temperature of outer thermocouple is kept as T_2 = 960 K. Nitrogen diluted hydrogen at room temperature (T_1 = 298 K) flows from the bottom duct, and a mini nozzle with an inner diameter of d = 2 mm produces a toroidal vortex that is strong enough to locally extinguish the flame on the burner centerline. The H_2/N_2 mixture that flows through the mini nozzle is identical to that of the main duct.

Nitric oxide and water vapor are introduced into the oxidizer stream. The NO doping is accomplished by replacing the N_2 in the oxidizer stream with a mixture of NO in N_2. Water vapor is added by flowing part of the oxidizer stream through a bubbler, that is maintained at a temperature of T_w = 333 K by a heated water reservoir. The temperature of the reservoir was monitored by a thermocouple. The water vapor in the bubbler is presumed to be saturated, and its partial pressure is calculated with following equation, $\log P_w(T) = G + A/T_w + B\cdot\log T_w + C\cdot T_w + D\cdot T_w^2 + E\cdot T_w^3 + F\cdot T_w^4$ where P_w is saturated vapor pressure in torr, T_w is the absolute temperature in K and A, B, C, D, E, F and G are constants, A = -2892.3693, B = -2.892736, C = -4.9369728×10^{-3}, D = 5.606905×10^{-6}, E = -4.645869×10^{-9}, F = 3.7874×10^{-12} and G = 19.3011421 [18]. To prevent the condensation of water vapor downstream of the bubbler, the water containing oxidizer is mixed with a dry oxidizer stream at the exit of the bubbler, and the flow lines that carry the water vapor are heated 10 K above the water temperature with an electric heater. The strain rate *a*, defined as the normal gradient of the normal component of

flow velocity on the oxidizer side of the stagnation plane is given by the expression $a = 2V_2/L\cdot(1+(V_1\cdot\rho_1{}^{0.5})/(V_2\cdot\rho_2{}^{0.5}))$ where L is a distance between the ducts, V is a normal velocity of the duct and ρ is the density of a stream [19]. The strain rate is kept constant at $a = 350\ s^{-1}$ for all experimental cases.

The extinction and re-ignition of the vortex-perturbed flame are imaged by measuring OH PLIF. The frequency-doubled output from a Nd:YAG pumped dye laser is tuned to 282.75 nm to pump the $Q_1 5$ line of the $A^2\Sigma^+ \leftarrow X^2\Pi^+$ ($v' = 1$, $v'' = 0$) band of OH. A 400 mm focal length cylindrical lens forms the laser beam into a vertical sheet through the reaction zone. The OH fluorescence is imaged onto an intensified CCD camera (512 × 512, Pixel Vision) with an *f/1.8* Cerco quartz camera lens. Color glass filters (UG-11 and WG-305) are used to block elastic scattering of the laser and transmit the OH fluorescence. The OH LIF measurements are performed in the linear LIF regime using laser energy of 0.6 mJ/pulse. The OH PLIF images are corrected for spatial variations in the laser sheet using acetone PLIF to measure the average beam profile.

Each extinction/ignition sequence begins by stabilizing a steady, flat counterflow flame on the burner. Subsequently, the speaker is pulsed to launch the vortex ring that impinges on the flame. The extinction/ignition events are highly repeatable, and different phases of the temporal evolution are measured by varying the delay time between the speaker pulse and the laser pulse with a digital delay generator. The repeatability also enables phase averaging of 10 ignition events to improve the signal-to-noise ratio. Radial profiles of the fuel duct inlet velocity are measured using molecular tagging velocimetry (MTV). For these measurements, acetone is seeded into the flow, and a pulsed ArF excimer laser (λ=193 nm) photodissociates the acetone along a narrow line located 1 mm above the duct exit. The excimer laser "writes" a line that is deficient in acetone. The location of the line is "read" by planar laser fluorescence (PLIF) imaging of acetone using the frequency-doubled dye laser for excitation. The resulting acetone PLIF image has a signal deficit along the line created by the excimer laser. This line is convected with the flow, and its displacement is measured from a pair of PLIF images that are acquired with different delay times between the excimer and dye lasers. The displacement distance is computed from the cross correlation of the two PLIF images, and the axial velocity is calculated by dividing the displacement distance by the time delay between the images. Velocities are measured for all phases of the pulsed flow. Figure 2 shows the temporal and spatial velocity variation of the pulsed mini-jet that forms the toroidal vortex.

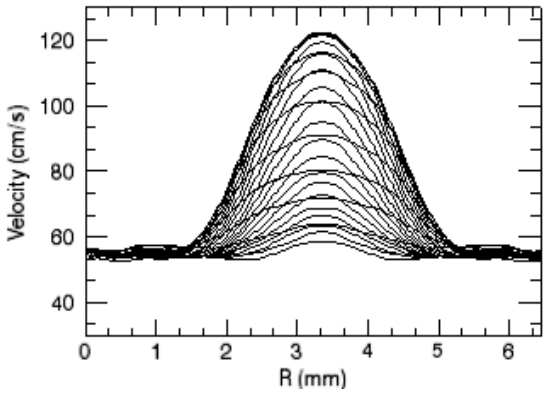

Figure 2: Temporal and spatial velocity variation of mini-jet measured using molecular tagging velocimetry

2.2 Numerical method

To numerically investigate the effects of NO and H_2O addition on extinction and re-ignition, direct numerical simulations of a vortex-perturbed hydrogen/air diffusion flame in axisymmetric counterflow were performed, using the in-house direct numerical simulation code, S3D, which solves the compressible Navier-Stokes, species continuity, and total energy equations. A fourth-order explicit Runge-Kutta method for time integration and an eighth-order central spatial differencing scheme were used [20,21] with a tenth-order filter to remove spurious high-wave number fluctuations. A detailed $H_2/O_2/NO_x$ kinetic mechanism [22] was used and CHEMKIN and TRANSPORT software libraries [23,24] were linked with S3D to evaluate reaction rates, thermodynamic and mixture-averaged transport properties.

The computational domain size is $L_x \times R$ = 12 mm × 12 mm with 400 grid points in each direction to resolve the flame and re-ignition structure. The fuel jet is hydrogen diluted with nitrogen ($X_{H2,1}$ = 0.115 and $X_{N2,1}$ = 0.885) at T_1 = 298 K, and the oxidizer is air at T_2 = 960 K, where subscripts 1 and 2 denote respectively the fuel and oxidizer streams. To study the affect of NO and water vapor on re-ignition, the oxidizer stream is doped with 160 ppm NO in Case 1 and with 2.6 % water vapor by volume and 160 ppm NO in Case 2. Steady inlet velocities for the simulations were imposed using the experimentally measured radial spatial velocity variation, where the overall strain rate based on the oxidizer stream is given by $a = 350\ s^{-1}$ [19].

Improved nonreflecting inflow/outflow boundary conditions for reacting counterflow simulations [25-28] were used for the inflow/outflow boundaries and symmetry conditions were specified at the burner axis. Details regarding the numerical configuration and boundary conditions are provided by Lee et al. [17]. An axisymmetric toroidal vortex, superimposed on the steady inlet velocities, is impulsively driven into the steady flame from the fuel stream boundary. Analytic functions are used to curve-fit the measured spatial and temporal velocity variations at the fuel inlet boundary. The evolution of the velocity profiles, measured using the MTV technique, are shown in Figure 2. Specifically, the velocity profiles are approximated by a combination of Gaussian, parabolic and tanh functions, and imposed at the fuel inlet boundary from the beginning of the simulation. The axial velocity component of the heated air stream is also measured and imposed at the oxidizer boundary of the simulation.

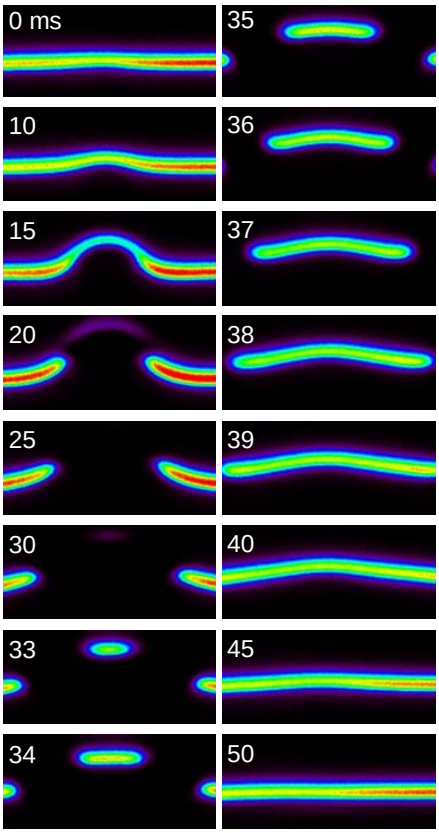

Figure 3: Sequence of OH PLIF images shows the extinction and re-ignition of a counterflow flame during an interaction with a pulsed vortex ring impinging from the fuel side (bottom). The fuel mixture is $X_{H2,1} = 0.115$, $X_{N2,1} = 0.885$, and the air is heated to $T_2 = 960$ K.

3. Experimental Results

3.1 Extinction and re-ignition of vortex perturbed hydrogen flame

We first consider extinction and re-ignition of a hydrogen counterflow flame without any additives in the reactant flows. In this experiment, a steady hydrogen flame is established with an air temperature of $T_2 = 960$ K, and is perturbed by a single fuel-side vortex. Figure 3 shows OH PLIF measurements of the temporal evolution of the flame-vortex interaction. At $t = 10$ ms, the flame starts to interact with the vortex, and at $t = 15$ ms, the vortex produces a large indent in the flame and the reaction zone becomes thinner near the centerline. Subsequently, this thinned region extinguishes and an annular edge-flame is established. After $t = 20$ ms, the diameter of the extinguished region gradually increases and autoignition occurs on the centerline at $t = 33$ ms. During the 33–36 ms period, the ignition kernel grows and the annular edge-flame retreats from the centerline until the edge-flame is completely extinguished. From $t = 37$ ms, the central ignition kernel grows until a flame is re-established across the image domain at approximately 40 ms. At $t = 50$ ms, a steady flat flame is re-established, indicating the completion of the flow perturbation. Previously, we have shown that the flame recovery process can occur in four different modes that involve different combinations of annular edge-flame propagation and the growth of an ignition kernel that forms on the centerline [17].

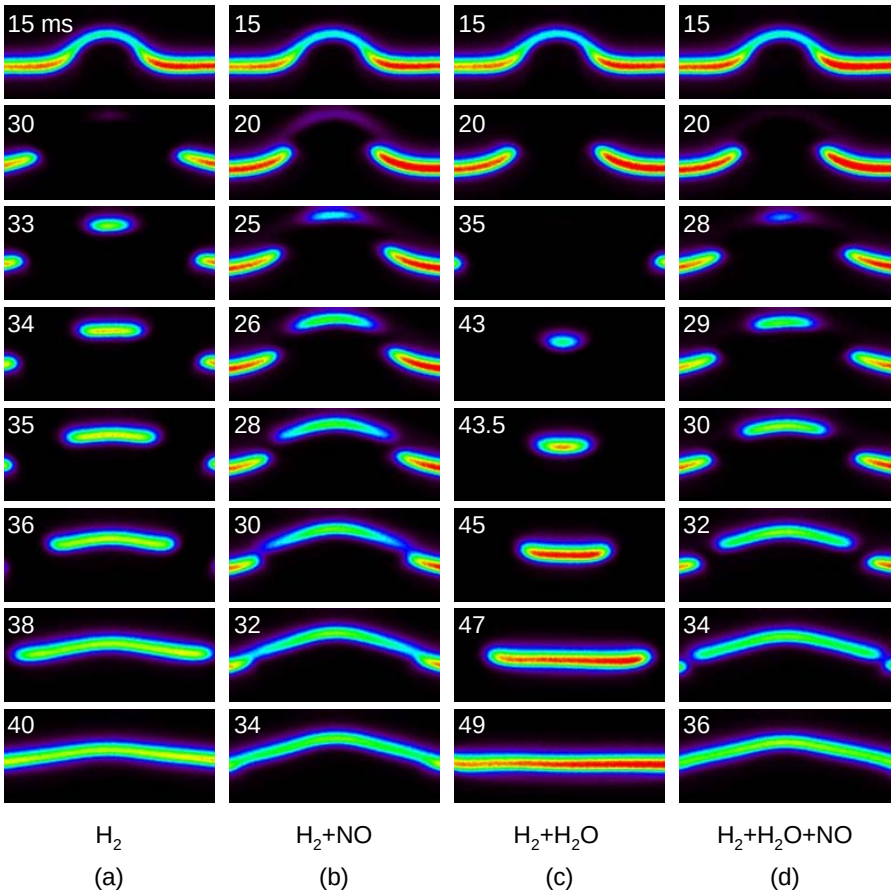

Figure 4: Sequence of recovery process during flame/vortex interaction. $X_{H2,1}$ = 0.115, $X_{N2,1}$ = 0.885, and T_2 = 960 K. (a) Hydrogen only (b) Hydrogen with NO (160 ppm) doping (c) Hydrogen with water vapor ($X_{H2O,2}$ = 0.012) (d) Hydrogen with water vapor ($X_{H2O,2}$ = 0.012) and NO

The mode of recovery is determined by the fuel composition, dilution level, oxidizer temperature, and the presence of additives. The recovery process displayed in Fig. 3 corresponds to Mode III in our previous results [17]. In this mode, the ignition kernel in the center recovers the extinguished region, and the retreating edge-flame extinguishes before the ignition kernel can merge with it.

3.2 Extinction and re-ignition with NO and H_2O

In previous work, we investigated the effects of oxidizer temperature, fuel concentration, and NO doping on the extinction and re-ignition properties of this system [17]. In the present study, the effects of water vapor and NO on extinction and re-ignition are investigated. Figure 4 shows the different recovery modes with and without the addition of water and NO. Figure 4a shows the extinction and re-ignition process without any additives and is a subset of the image sequence in Fig. 3. Figure 4b shows the effect of NO doping on the flame response. A comparison of Figs. 4a and 4b reveals that NO doping causes the flame to recover by the merging of the central re-ignition kernel and the annular edge-flame. This mode of recovery was designated as Mode IV in our previous study [17].

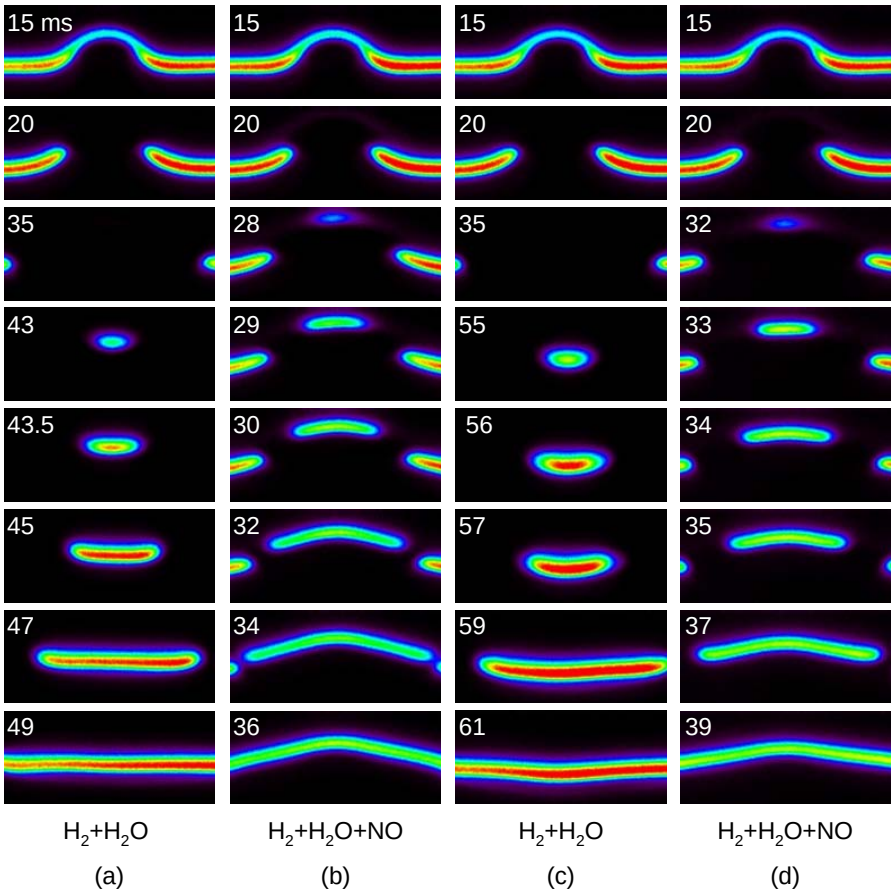

Figure 5: Sequence of recovery process during flame/vortex interaction. $X_{H2,1}$ = 0.115, $X_{N2,1}$ = 0.885, and T_2 = 960 K. (a) Hydrogen with water vapor ($X_{H2O,2}$ = 0.012) (b) Hydrogen with water vapor ($X_{H2O,2}$ = 0.012) and NO (c) Hydrogen with water vapor ($X_{H2O,2}$= 0.018) (d) Hydrogen with water vapor ($X_{H2O,2}$ = 0.018) and NO

As a result of the catalytic effect of NO, the central autoignition kernel forms at an earlier time, which increases the probability of merging between the autoignition kernel and retarding edge-flame. This combination of ignition processes decreases the flame recovery time by more than 6 ms compared to the case without NO (Fig. 4a). Figure 4c shows that the addition of 1.2% water vapor by volume can significantly change the recovery of the flame. In this case, the water vapor inhibits the ignition process until the annular edge-flame completely disappears and the flame is fully extinguished during t = 36–42 ms. At t = 43 ms, re-ignition occurs near the centerline, and the ignition kernel expands until the entire flame is re-ignited. The total flame recovery time is significantly longer than the case without water (Fig. 4a). Note that the curvature of the re-ignition kernel is opposite to those of other cases since the re-ignition kernel in Fig. 4c is initiated by the relaxation of strain rate after the vortex dissipates. Figure 4d shows the flame response with both water vapor and NO. Due to the combination of the NO catalytic effect and the H_2O inhibiting effect, the induction time for the autoignition is between the water vapor addition case (Fig. 4c) and NO doping case (Fig. 4b). This flame shows the same recovery mode as Fig. 4a, but the total recovery time is much shorter because the catalytic effect of NO dominates over the inhibiting effect of water.

Figure 5 shows the effect of increasing the water mole fraction in the oxidizer stream by 50 %. The water mole fraction for Figs. 5a and 5b is $X_{H2O,2} = 0.012$ and that of Fig. 5c and 5d is $X_{H2O,2} = 0.018$. For each condition of water mole fraction, the left series of images (Fig. 5a and 5c) shows the flame recovery without NO doping, and the right series (Fig. 5b and 5d) shows the re-ignition with NO. The similarity of the images at 15 ms and 20 ms for all four conditions indicates that these relatively low water concentrations have a negligible impact on the extinction phase of the vortex-flame interaction. However, the timing of the re-ignition process is significantly modified by the water. A comparison of Figs. 5a and 5c shows that increasing the water mole fraction without any NO doping delays the autoignition kernel formation by approximately 12 ms. In contrast, the autoignition is delayed by only 4 ms from Fig. 5b to Fig. 5d, indicating that NO doping reduces the impact of the additional water. The NO doping advances the autoignition time by 15 ms and 23 ms for the water mole fractions $X_{H2O,2} = 0.012$ and $X_{H2O,2} = 0.018$, respectively. The earlier onset of ignition significantly shortens the overall flame recovery time. The flame recovery process for $X_{H2O,2} = 0.018$ (Fig. 5d) is very similar to that of the no-additive case (Fig. 4a), which implies the inhibition effect of water vapor counterbalances the catalytic effect of NO.

3.3 Effect of water vapor on extinction and re-ignition

The effect of water vapor on the flame recovery is further investigated by repeating the vortex-flame experiments over a wider range of water mole fraction. Figure 6 shows the change of flame response for water mole fractions ranging from $X_{H2O,2} = 0.012$ to 0.071. For all conditions, the oxidizer is doped with 160 ppm of NO. The flame is unable to recover without the NO doping if the water mole fraction is larger than $X_{H2O,2} = 0.018$.

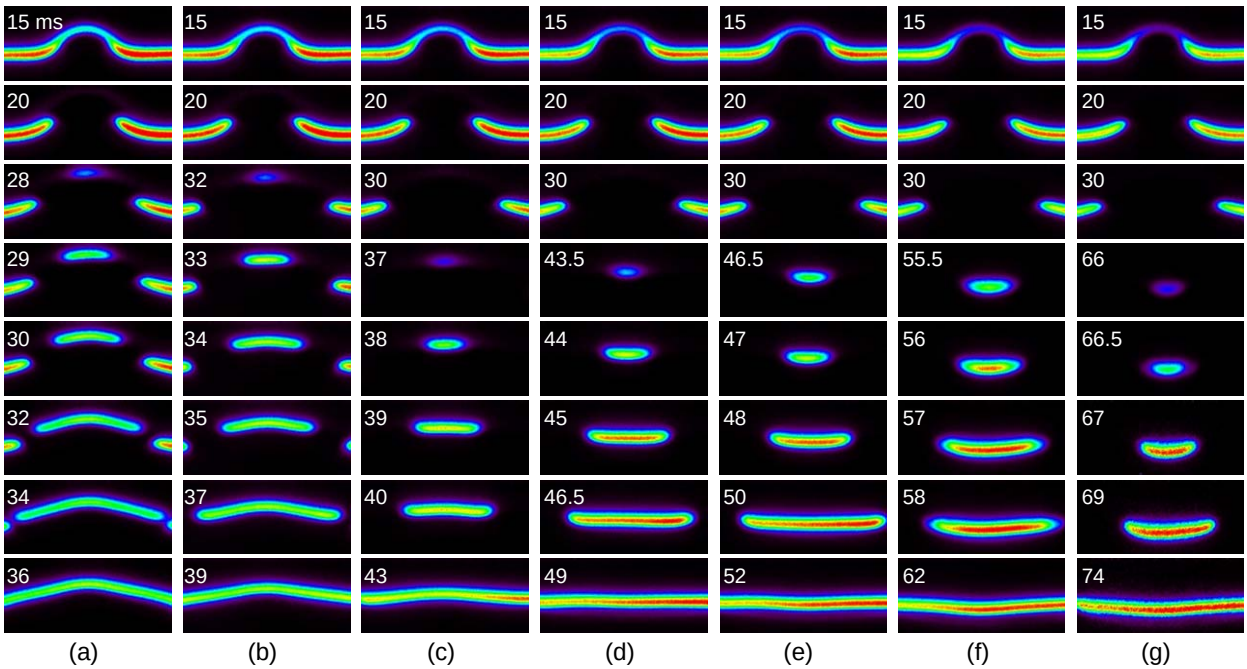

Figure 6: Sequence of recovery process of hydrogen flame with water vapor and NO doping. $X_{H2,1}$ = 0.115, $X_{N2,1}$ = 0.885, T_2 = 960 K, and $X_{NO,2}$ = 160 ppm. (a) $X_{H2O,2}$ = 0.012 (b) $X_{H2O,2}$ = 0.018 (c) $X_{H2O,2}$ = 0.026 (d) $X_{H2O,2}$ = 0.034 (e) $X_{H2O,2}$ = 0.04 (f) $X_{H2O,2}$ = 0.055 (g) $X_{H2O,2}$ = 0.071

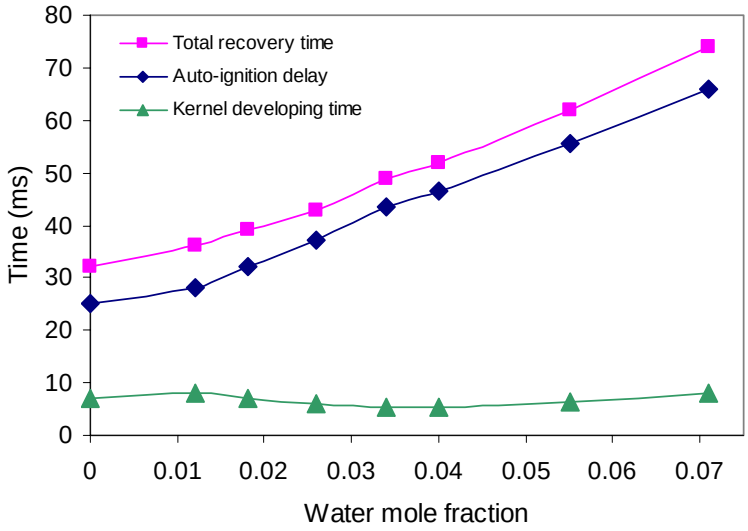

Figure 7: Autoignition delay, Total recovery time and Kernel developing time with respect to water mole fraction. $X_{H2,1}$ = 0.115, $X_{N2,1}$ = 0.885, T_2 = 960 K, and $X_{NO,2}$ = 160 ppm.

With NO doping, the flame can re-ignite for water mole fractions up to $X_{H2O,2} = 0.071$. Images at t = 15 ms and 20 ms of each case show the effect of water vapor on extinction. The OH LIF signal of the indented region as well as the region outside the vortex-perturbed area decreases as the water mole fraction increases, but the position of the annular edge-flames at 20 ms are almost identical for the different water mole fractions. This result implies that this amount of water vapor has little effect on the edge-flame formation and propagation.

However, the water vapor can give a great impact on the formation of the autoignition kernel. The increase of water vapor retards the formation of autoignition kernel which results in the transformation of the flame recovery mode. In Figs. 6a and 6b, the autoignition occurs while the edge-flame is retreating (Mode III), but in Figs. 6c–6g the autoignition occurs after the edge-flame is completely extinguished (Mode II). Figure 7 shows the autoignition delay, total recovery time and kernel developing time as a function of water mole fraction. The kernel developing time is the elapsed time from the initiation of the kernel to the formation of a fully expanded flame (i.e. the difference between total recovery time and autoignition delay time). Note that the ignition delay and total recovery time are proportional to water mole fraction, but the kernel developing time is relatively invariant which means the increase of the recovery time mainly results from the autoignition delay rather than from any change of the propagation speed of the ignition kernel. Note that the ignition delay of the maximum water content condition is approximately 40 ms longer than the case without water addition.

The axial location and curvature of the ignition kernels varies with the concentration of the added water vapor. In Figs. 6a-c, the ignition kernels are concaved toward the fuel-side while they are concaved to the air-side in Figs. 6d-g. The OH-LIF signal in the ignition kernel increases from Fig. 6a to 6d . This variation may be partially the result of a reduced strain rate for the ignition kernels that form at later times. .The effect of the physical parameters and chemical effect of water on autoignition phenomena will be discussed in the next section.

4. Numerical Results

To understand the effects of NO and water vapor addition on extinction and re-ignition in more detail, we simulated the transient interaction of a flame with a vortex that was impulsively driven into the flame from the fuel stream. Two typical cases are chosen to compare with the experiments: for Case 1, 160 ppm NO is added to the oxidizer stream and for Case 2, 2.6 % water vapor by volume and 160 ppm NO are included.

The temporal evolution of X_{OH} for the two cases is presented in Fig. 8 to show the overall effects of NO and water vapor addition. The extinction/re-ignition in Case 1 occurs faster than in Case 2, as in the experimental results. However, the time required for the extinction/re-ignition process in the simulations is longer than in the experiments by 5–7 ms. This discrepancy may result from the sensitivity of extinction/re-ignition timing to the chemical mechanism and the uncertainties in measured temperatures and velocities.

The computational results show that the local extinction/re-ignition occurs along the burner axis, as it does in the experiments. Figure 9 shows the temporal evolution of the maximum temperature and the scalar dissipation rate, χ, at the location of maximum OH mole fraction along the burner axis for the two cases. The scalar dissipation rate at the location of maximum OH mole fraction is chosen to represent the mixing rate at the reaction zone. This choice is deemed more appropriate than using the location of stoichiometric mixture fraction, which lies outside of the reaction zone in this highly diluted hydrogen/air nonpremixed flame [29].

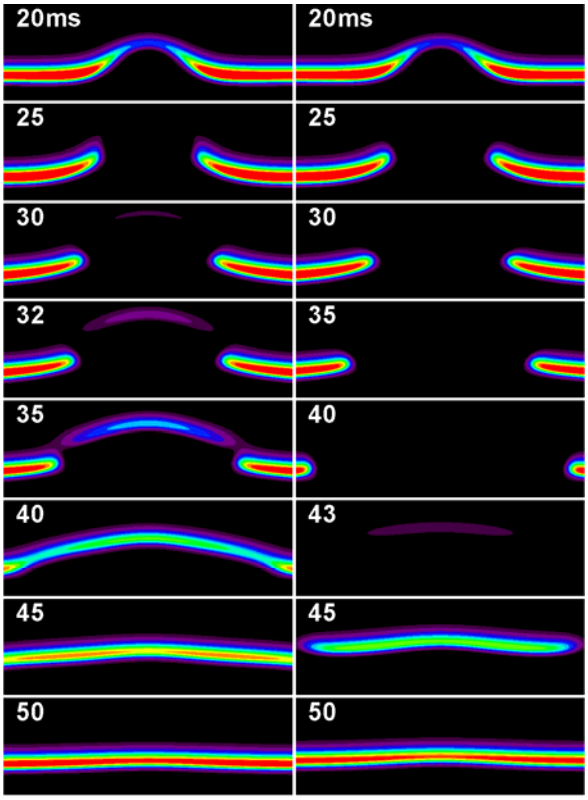

Figure 8: Temporal evolution of OH mole fraction isocontours for Cases 1 and 2.

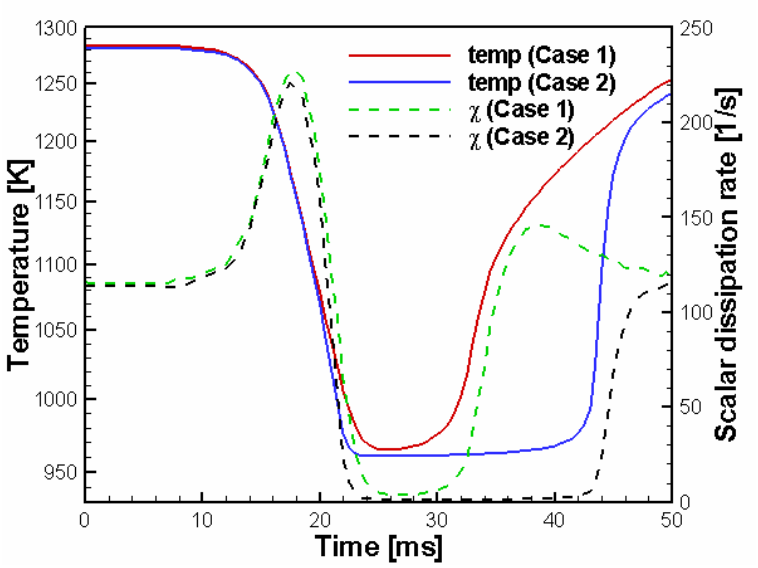

Figure 9: Temporal evolution of maximum temperature and scalar dissipation rate at maximum OH location along the burner axis for Cases 1 and 2.

The vortex that is injected from the fuel stream thins the reaction zone by pushing the cold fuel stream towards the oxidizer stream. The dissipation rate increases, reaching a maximum value in excess of 200 s^{-1}, and the temperature decreases in concert. As a result, the flame is locally extinguished and a circular flame hole is generated in the center region at approximately 22ms for both cases. At a later time, the quenched flame hole is recovered by re-ignition from the center as the high χ is relaxed.

However, it is of interest to note that the peak χ related to the extinction is much less than the extinction scalar dissipation rate, χ_q of corresponding strained laminar nonpremixed flame: the maximum χ_q is 660 s^{-1} and χ_q at the maximum OH location 362 s^{-1} from OPPDIF [30]. This result implies that the extinction occurs not only by high compressible strain rate represented by χ but also by the other effects such as curvature and differential diffusion as mentioned in the previous section. It is found that the defocusing effect of hydrogen by its high differential diffusion at the tip of the vortex weakens the flame and thus, the flame is readily quenched by local χ weaker than χ_q. From numerous simulations, it is also found that the flame is liable to be quenched by a particular shape of vortex rather than by the vortex strength. In other words, the flame can overcome even a strong vortex of which shape is top-hat at the inlet boundary but it is readily quenched even by a weak vortex with a parabolic shape. This means that the differential diffusion of hydrogen related to curvature is another key factor to induce local flame extinction.

To understand the chemical effect of NO and water vapor addition on extinction/re-ignition, the elementary reactions involved in the process were analyzed. Figure 10 shows the temporal evolutions of OH and HO_2 mole fractions and selected elementary reactions at the maximum OH location along the polar axis for Cases 1 and 2.

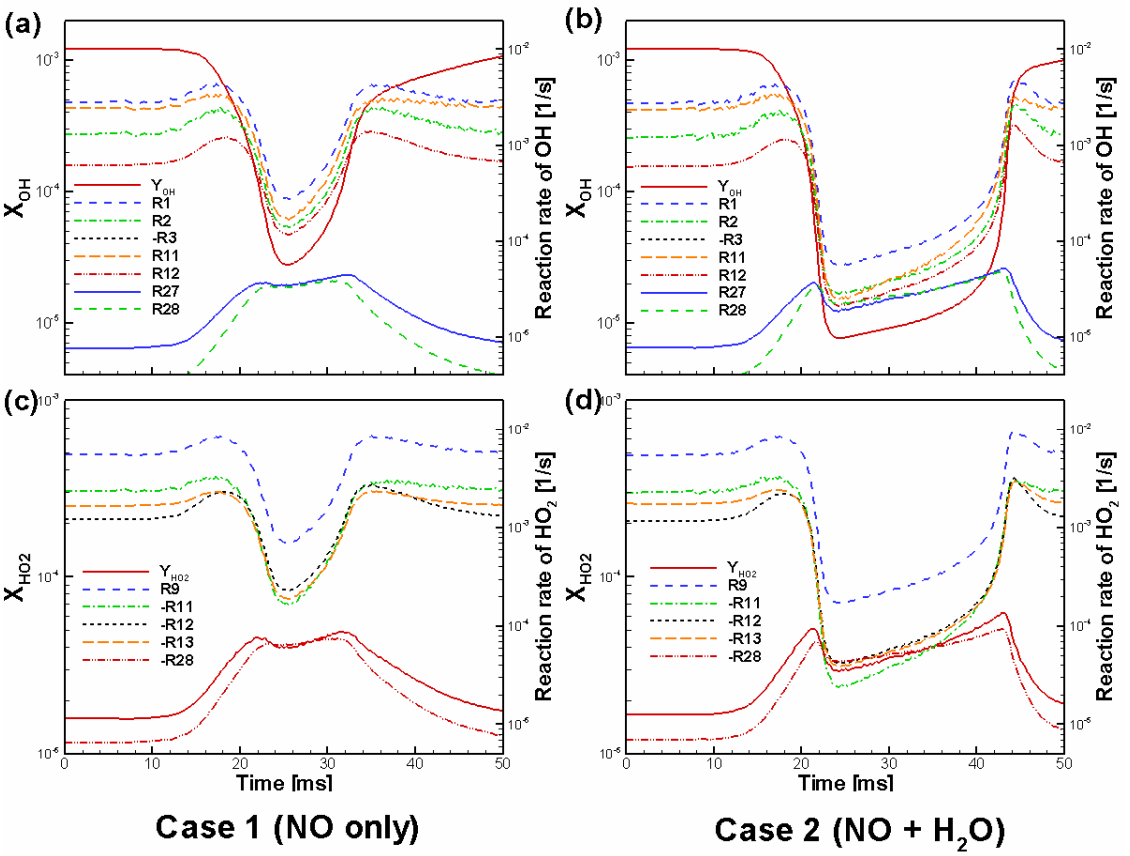

Figure 10: Temporal evolution of the mole fractions and elementary reaction rates of OH (top) and HO_2 (bottom) at the maximum OH location along the burner axis for Case 1 (left) and Case 2 (right).

Readers are referred to Table 1 for selected elementary reactions involved in the $H_2/O_2/NO_x$ chemistry. Until the local flame quenching, the temporal behaviors of the mass fractions and reaction rates are very similar to each other for two cases. However, after around 22ms, the values in Case 1 bound back and finally re-ignition occurs but the values in Case 2 drop down significantly compared to Case 1 and then keep growing slowly until re-ignition occurs at 43 ms.

Table 1: Selected elementary $H_2/O_2/NO_x$ reactions (Units are cm^3-mol-s-kcal-K, and $k = AT^n \exp(-E/RT)$ from Ref [22])

			A	*N*	*E*
R1 :	$H + O_2$	= $O + OH$	3.547E+15	-0.406	1.6599E+04
R2 :	$H_2 + O$	= $OH + H$	0.508E+05	2.670	0.6290E+04
R3 :	$OH + H_2$	= $H + H_2O$	0.216E+09	1.510	0.3430E+04
R9 :	$O_2 + H + M$	= $HO_2 + M$	1.475E+12	0.600	0.0000E+00
R11:	$H + HO_2$	= $OH + OH$	7.079E+13	0.000	2.9500E+02
R12:	$O + HO_2$	= $OH + O_2$	3.250E+13	0.000	0.0000E+00
R13:	$OH + HO_2$	= $O_2 + H_2O$	2.890E+13	0.000	-4.9700E+02
R27:	$H + NO_2$	= $OH + NO$	1.320E+14	0.000	3.6200E+02
R28:	$NO + HO_2$	= $OH + NO_2$	2.110E+12	0.000	-4.7900E+02

It is also of interest to note that even though R27 and R28 related to the NO catalytic cycle [8–12, 15–17] are smaller than the other reactions; they have their peak between the extinction and re-ignition in both cases unlike the other reactions. This means that the small amount of NO addition enhances reaction during the induction period by consuming HO_2 and generating OH via R27 and R28 which form a catalytic cycle as mentioned in the introduction. However, water vapor addition generates more HO_2 via the recombination reaction, R9 such that the ignition delay time is increased with the amount of water vapor addition. Figure 11 shows the temporal evolutions of the reaction rate and mass fraction of HO_2 at maximum OH location for two cases. Until the local extinction, the reaction rate of HO_2 in Case 2 is slightly greater than in Case 1 and thus accumulated HO_2 mass fraction in Case 2 is also greater than in Case 1. This difference in HO_2 reaction rate and mass fraction of the two cases results in the large difference in the ignition delay time as shown in Fig. 8.

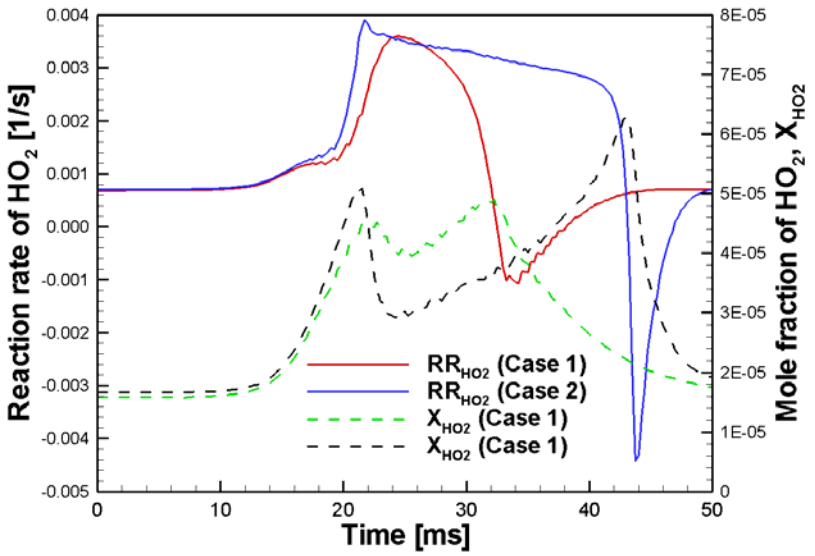

Figure 11: Temporal evolution of reaction rate and mole fraction of HO_2 at maximum OH location at the burner axis for Cases 1 and 2.

5. Concluding Remarks

The effect of water vapor and NO addition on the extinction and re-ignition of a vortex-perturbed hydrogen diffusion flame were studied in a heated counter-flow configuration. For constant air temperature and vortex strength, the extinction and recovery behavior were measured in terms of water vapor mole fraction with and without NO doping. The addition of a small amount of NO enhanced re-ignition and helped to maintain the flame while water vapor inhibited the onset of autoignition. Increased concentration of water vapor retarded the formation of an autoignition kernel which controlled the total recovery time and recovery mode. A small amount of NO enlarged the upper limit of water vapor content for controlling the system, enabling the variation of autoignition delay up to 40 ms. This result demonstrates the utility of water-NO mixtures as an effective ignition-controlling agent in practical applications, including hydrogen-air combustion systems with exhaust gas recirculation.

To understand the details of NO and water vapor effects on the extinction/re-ignition process, direct numerical simulations of a vortex-perturbed hydrogen diffusion flame were performed using experimentally measured temporal and spatial profiles of the inlet velocities. The numerical results showed that the local flame quenching resulted from the high scalar dissipation rates induced by the vortex and the differential diffusion of hydrogen at the tip of the vortex. An elementary reaction rate analysis confirmed that NO doping enhances OH generation by forming a catalytic cycle via reactions R27 and R28 during the induction period, and a small amount of water vapor can counteract this catalytic process and significantly retard the ignition delay time.

It is remarkable that water vapor has a minimal effect on the extinction and edge-flame propagation, but has significant impact on the formation of an autoignition kernel. Given that the chemical inhibition effect of water vapor acts primarily through its important role as a third-body chaperon efficiency in the recombination reaction $H + O_2 + M = HO_2 + M$, it is not surprising that a high-temperature flame phenomenon, such as edge propagation, is unaffected by water vapor since the importance of this recombination reaction diminishes above 1350 K. It suggests that accurate chemical mechanisms for ignition are very important for accurate modeling of a combustion system whose ignition process is very sensitive to the additives such as water vapor and NO.

Acknowledgments

We thank Prof. F. L. Dryer of Princeton University for providing the $H_2/O_2/NO_x$ chemical mechanism and for suggesting the investigation of NO doping in strained ignition studies. We gratefully acknowledge R. J. Sigurdsson of Sandia National Laboratories for assistance in the laboratory. This research was supported by the U.S. Department of Energy, Office of Basic Energy Sciences, Division of Chemical Sciences, Geosciences, and Biosciences. Sandia National Laboratories is a multiprogram laboratory operated by Sandia Corporation, a Lockheed Martin Company, for the U.S. Department of Energy under contract DE-AC04-94-AL85000.

References

[1] C. M. White, R. R. Steeper, A. E. Lutz, *Int J Hydrogen Energy* 31 (2006) 1292-1305.
[2] F. Halter, C. Chauveau, N. Djebïli-Chaumeix, I. Gökalp, *Proceedings of the Combustion Institute* 30 (2005) 201-208.
[3] C. Mandilas, M. P. Ormsby, C. G. W. Sheppard, R. Woolley, *Proceedings of the Combustion Institute* 31 (2007) 1443-1450.
[4] F. Halter, C. C. Chauveau, I. Gökalp, *Int J Hydrogen Energy* 32 (2007) 2585-2592.
[5] G. S. Jackson, R. Sai, J. M. Plaia, C. M. Boggs, K. T. Kiger, *Combustion and Flame 132* (2003) 503-511.
[6] D. D. S. Liu, R. MacFarlane, *Combustion and Flame* 49 (1983) 59-71.
[7] R. Seiser, K. Seshadri, *Proceedings of the Combustion Institute* 30 (2005) 407-414.
[8] W. R. Laster, P. E. Sojka, *Journal of Propulsion* 5 (1989) 385-390.
[9] Y. Tan, C. G. Fotache, C. K. Law, *Combustion and Flame* 119 (1999) 346-355.
[10] C. J .Sung, J. G. Li, G. Yu, C. K. Law, *AIAA Journal* 37 (1999) 208-214.
[11] M. A. Mueller, R. A. Yetter, F. L. Dryer, *International Journal of Chemical Kinetics* 31 (1999) 705–724.
[12] M. A. Mueller, R. A. Yetter, F. L. Dryer, *International Journal of Chemical Kinetics* 32 (2000) 317–339.
[13] P. Dagaut, F. Lecomte, J. Mieritz, P. Glarborg, *International Journal of Chemical Kinetics* 35 (2003) 564-575.
[14] G. Dayma, P. Dagaut, *Combustion Science and Technology* 178 (2006) 1999-2024.
[15] F. L. Dryer, *Private Communication*, 2006.
[16] P. Risberg, D. Johansson, J. Andrae, G. Kalghatgi, P. Björnbom, H. E. Ångström, *SAE Technical Paper Series* 2006-01-0416.
[17] U. D. Lee, S. A. Kaiser, C. S. Yoo, J. H. Chen, J. H. Frank, *5th US Combustion Meeting San Diego CA, Paper #A05* (2007)
[18] M. Parks, D. Watling, *Pharamaceutical Technology Europe* 01 March (2004)
[19] K. Seshadri, F. A. Williams, *International Journal of Heat and Mass Transfer* 21 (1978) 251–253.
[20] C. A. Kennedy, M. H. Carpenter, *Applied Numerical Mathematics* 14 (1994) 397–433.
[21] C. A. Kennedy, M. H. Carpenter, R. M. Lewis, *Applied Numerical Mathematics* 35 (2000) 177–264.
[22] F. L. Dryer, *Private Communication*, 2006.
[23] R.J. Kee, F.M. Rupley, E. Meeks, J.A. Miller, *CHEMKIN-III: A Fortran Chemical Kinetics Package for the Analysis of Gas-Phase Chemical and Plasma Kinetics*, Tech. Rep. SAND96-8216, Sandia National Laboratories, 1996
[24] R.J. Kee, G. Dixon-Lewis, J. Warnatz, M.E. Coltrin, J.A. Miller, *A Fortran Computer Code Package for the Evaluation of Gas-Phase Multicomponent Transport Properties*, Tech. Rep. SAND86-8246, Sandia National Laboratories, 1986.
[25] C. S. Yoo, H. G. Im, *Proceedings of the Combustion Institute* 30 (2005) 349–356.
[26] C. S. Yoo, Y. Wang, A. Troué, H. G. Im, *Combustion Theory and Modelling* 9 (2005) 617–646.
[27] C. S. Yoo, H. G. Im, *Combustion Theory and Modelling* 11 (2007) 259–286.
[28] C. S. Yoo, H. G. Im, *Proceedings of the Combustion Institute* 31 (2007) 701–708.
[29] C. S. Yoo, J. H. Chen, J. H. Frank, *5th US Combustion Meeting San Diego CA, Paper #A01* (2007)
[30] A.E. Lutz, R.J. Kee, J.F. Grcar, F.M. Rupley, OPPDIF: A Fortran Program for Computing Opposed–Flow Diffusion Flames, Tech. Rep. SAND96-8243, Sandia National Laboratories, 1997.